

# Edge magnetoplasmons in a partially screened two-dimensional electron gas on a helium surface

M. I. Goksu,<sup>1,2</sup> M. okyang R. K. in,<sup>1</sup> K. A. M. antey,<sup>1,y</sup> and A. J. D. ahm<sup>1</sup>

<sup>1</sup>Department of Physics, Case Western Reserve University, Cleveland, Ohio 44106-7079, USA

<sup>2</sup>Truman State University Science Division, 100 East Normal Street, Kirksville, Missouri 63501 USA

(Dated: October 23, 2006)

We report a study of edge magnetoplasmons in a partially-screened system of electrons on a helium surface. We compare experimental results with theories of the frequency, damping, and penetration-depth dependence on magnetic field, temperature-dependent damping, and the dependence of the frequency on screening. We show explicitly the dependence of frequency on the edge density profile. The frequency and screening are in qualitative agreement with the theory of Fetter at small fields, and the frequencies agree with theory in the limit of zero magnetic field. The frequency and linewidths in intermediate and large fields exhibit the features of the qualitative predictions of Volkov and Mikhailov, but differ numerically. Deviations from theory for a finite sample occur at smaller fields. The dependence of frequency on the density profile is stronger than predicted by these authors, and the penetration-depth variation with field confirms their prediction for small fields.

PACS numbers: 73.20.Mf

## I. INTRODUCTION

Edge magnetoplasmons (EMPs) are plasma modes that propagate around the perimeter of a two-dimensional (2D) array of charges. A degenerate mode at zero magnetic field splits into two modes at finite B fields. The frequency of one mode increases with field, while the frequency of the EMP mode decreases. The penetration depth of the upper mode increases with field and becomes infinite at a finite value of B, thereby becoming a bulk 2D mode. The penetration depth of the lower mode decreases with increasing B.

Edge magnetoplasmons were first detected in a partially-screened array of electrons on a helium surface by Mast et al. [1, 2] and by Gattli et al. [3]. Screening is provided by metallic plates located above and below the electron layer and is described by a screening length, which depends on the separation of the sample from these plates. Both groups developed theories, with which they compared their data. Earlier modes observed in a quantum dot [4] have since been interpreted as EMP modes. Edge modes have been investigated extensively in 2D semiconductor samples.

Gattli et al. [5] extended their studies to low and intermediate magnetic fields. Peters et al. [6] and Monarkha et al. [7] measured the damping of these modes at high magnetic fields. Studies of EMPs at a density discontinuity have been studied by Sommerfeld et al. [8]. Experimental studies of related acoustic edge modes with  $n$  radial nodes ( $n > 1$ ) have been made on electron [9, 10, 11] and ionic [12] arrays at the surface of liquid helium.

Edge modes in a sample of electrons on a helium surface have been treated theoretically by a number of authors. [13, 14, 15, 16, 17, 18, 19, 20] Here we present a study of EMP modes in a partially screened system in a circular sample for small and intermediate fields and compare them with theories by Fetter [15] and Volkov and Mikhailov. [16, 17] Preliminary work has been presented elsewhere. [21, 22]

## II. THEORY

Fetter [15] solved for the edge magnetoplasmon modes of a 2D electron array in a circular sample of radius  $R$  located symmetrically between two metallic plates each located a distance  $h$  from the electron layer. A magnetic field is applied along the  $z$  axis normal to the layer. A step density profile at the sample perimeter was assumed. He solved a hydrodynamic model of a compressible charged fluid placed in a uniform neutralizing background. The continuity and Euler equations that describe the dynamics are

$$\partial n_r / \partial t + \nabla_r \cdot \mathbf{v} = 0; \quad (1)$$

$$\partial \mathbf{v} / \partial t + c^2 \nabla_r \cdot \mathbf{n} - (e/m) r \cdot \nabla \phi = 0; \quad (2)$$

where  $n_r$  is the local electron density,  $n$  is the average electron density,  $\mathbf{v}$  is the local velocity of the electron fluid,  $c$  is the effective wave speed that allows for dispersion in the propagating wave,  $\phi$  is the electrostatic potential at the plane of the charges ( $z = 0$ ),  $\omega_c$  is the cyclotron frequency, and  $\nabla_r$  is the two-dimensional gradient operator. Poisson's equation relates the potential and the charge density;

$$\nabla_r^2 \phi = n_r - n_0; \quad (3)$$

Present address: Department of Physics, California State University-Dominguez Hills, Carson, CA 90747, USA

<sup>y</sup>Present address: Department of Physics, University of Illinois, Urbana, IL 61801-3080, USA

A solution of the form  $e^{(i\mathbf{q} \cdot \mathbf{r} - i\omega t)}$ , where  $\mathbf{q}$  lies in the  $xy$  plane, is substituted into these equations and boundary conditions are applied. With a Hankel transform of the potential and neglect of the sound velocity for long wavelengths, Fetter arrives at the following equations to be solved for the resonance frequencies.

$$\sum_{j=0}^{\infty} [K_{ij} - \left(\frac{i}{\omega_0} - \frac{i}{\omega_c}\right)^2 g_{ij}] c_j = 0; \quad (4)$$

Here,

$$\omega_0^2 = \frac{ne^2 \tanh(h=R)}{m R_0 (\epsilon + 1)}; \quad (5)$$

where  $\epsilon$  is the dielectric constant of liquid helium. The kernel matrix  $K_{ij}$  is defined as

$$K_{ij} = \coth\left(\frac{h}{R}\right) \frac{d}{dp} \tanh\left(\frac{ph}{R}\right) J_{L+2i+1}(p) J_{L+2j+1}(p); \quad (6)$$

where  $J(p)$  is a Bessel function, and  $L = |k|$  is an integer;  $k$  is the azimuthal mode number. The matrix  $g_{ij}$  has only the single nonzero element

$$g_{00} = [\beta L (L+1)^2]^{-1}; \quad (7)$$

The matrix element  $g_{ij}$  is symmetric and tridiagonal with nonzero elements,

$$g_{ii} = [4(L+2i)(L+2i+1)(L+2i+2)]^{-1}; \quad (8)$$

$$g_{i,i+1} = [\beta(L+2i+1)(L+2i+2)(L+2i+3)]^{-1}; \quad (9)$$

Volkov and Mikhailov [16, 17] used the Wiener-Hopf method to solve Eqs. (1)–(3). These authors defined the penetration depth of the EMP mode into the sample as the largest of  $h$ , the width of the density profile  $b$ , and a magnetic length  $\lambda$ . For small  $qh$ ,  $\lambda^2 \approx \lambda_c^2$ , and  $\lambda \approx \lambda_c$ ,  $\lambda$  is given by

$$\lambda = \frac{ne^2}{m \omega_0 (\epsilon + 1) \lambda_c^2}; \quad (10)$$

Here  $q$  is the azimuthal wave vector, and  $\lambda$  is the scattering time for  $B = 0$ . Since the lengths  $h$  and  $b$  are nearly equal for our sample, we take for our analysis

$$\lambda = (\lambda^2 + b^2)^{1/2}; \quad (11)$$

For the circular geometry used in this experiment these authors find

$$\begin{aligned} \lambda_L &= \frac{x_{xy} q}{\omega_0 (\epsilon + 1)} = \frac{neL}{\omega_0 (\epsilon + 1) RB}; \\ &= \ln \frac{2R}{\lambda} \left( L + \frac{1}{2} \right) + 1; \end{aligned} \quad (12)$$

where  $x_{xy}$  is the Hall conductivity, and  $\gamma$  is the digamma function. This formula was derived for a step density profile and  $\lambda \gg R$ , which for our system requires  $B \approx 10^3$

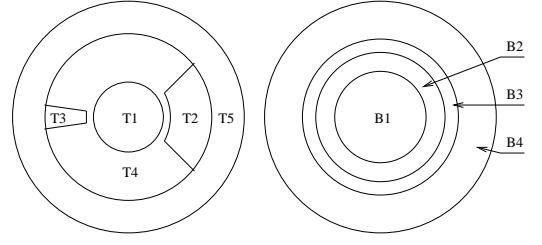


FIG. 1: Configuration of electrodes located above and below the electron layer. The electrodes in the top T and bottom B plates are described in the text.

T. For a finite density profile width we have substituted  $\lambda$  in their argument of the logarithm.

These authors also obtain a formula that includes the density profile ( $x=h$ ) for a semi-infinite plane, where  $x$  is measured from the edge of the sample. Adapting their formula to a circular geometry as an approximation by setting  $q = L/R$ , the frequency is obtained with a screening length of  $h=2$  as

$$\begin{aligned} \lambda_L &= \frac{x_{xy} q}{\omega_0 (\epsilon + 1)} = \frac{neL}{RB \omega_0 (\epsilon + 1)}; \\ &= \left[ \ln \frac{2h}{b} + A \right]; \\ A &= \frac{1}{d} \ln \left( \frac{1}{\epsilon} \right) \frac{\epsilon}{\epsilon} \end{aligned} \quad (13)$$

This equation was derived under the conditions  $h=R$  and  $b=h$ .

Shikin's and Nazin [20] included the density profile by solving Eqs. (1)–(3) numerically for the case of specific density profiles in a circular geometry.

Volkov and Mikhailov [17] derived the linewidth of the modes for a semi-infinite plane and  $\lambda \gg 1$ . We adapt their formula by substituting  $q = L/R$ ;

$$\lambda_L = \frac{1}{\lambda_L} \frac{neL}{\omega_0 (\epsilon + 1) RB}; \quad (14)$$

### III. EXPERIMENTAL SETUP

Our sample cell consists of a plane-parallel circular capacitor with a plate separation of 2 mm. Electrons are deposited on a helium surface located midway between the plates. The capacitor plates are made of copper-clad epoxy board, and electrodes are etched on the inner side of each plate. Voltages are applied on these electrodes to excite EMP modes and to fix the radius and density of the electron pool.

The electrode configuration is shown in Fig. 1. The bottom plate is separated into four concentric electrodes of outer radii 5.8, 8.2, 10, and 13 mm. The top plate includes three electrodes on which a rf voltage is applied to drive resonant modes. The inner circular electrode  $T_1$

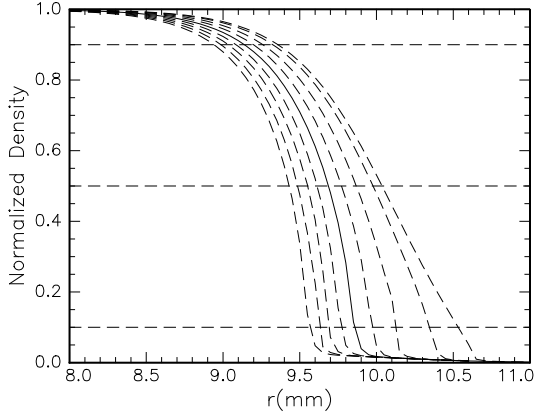


FIG. 2: Density profiles for different ratios of guard to holding voltages. The ratios of  $V_g/V_h$  are from left to right 0.8; 0.7; 0.6; 0.5; 0.4; 0.3; 0.2; 0.1; 0.05

is used for radial modes, and two electrodes  $T_2$  and  $T_3$  spanning angles of  $80^\circ$  and  $12^\circ$ , respectively, are used to drive EMP modes. A larger electrode  $T_4$  is used in conjunction with electrodes in the lower plate as a capacitor plate to measure the helium level. A guard voltage  $V_g$  is applied to electrodes,  $T_5$  and  $B_4$ , and to a 2 mm high circular electrode just beyond these to confine the sample and shape the electron density profile. For smaller pool radii the guard voltage is also applied to one or two of the inner circular electrodes in the bottom plate.

We work at the saturated density  $n = V_h / \phi_0 e h$ . The melting temperature serves as a check on the density and helium level. We estimate the density values to be accurate to within 5%.

A broadband, homodyne, rf reflection spectrometer is used to detect the power absorbed as a function of frequency. A 50  $\Omega$  coax line is terminated in a 50  $\Omega$  resistor in parallel with the driving electrode. A line of equivalent electrical length is added to the reference arm of the spectrometer. Both arms of the spectrometer have identical components so that there is no relative phase shift as the frequency is swept. The electron density and the radius of the pool are modulated by an audio-frequency voltage applied to the guard electrodes for phase-sensitive detection. The cell is leveled by maximizing the steepness of the mobility change at the melting transition of the sample.

The radius and width of the sample profile are determined by a numerical simulation. Profiles are shown in Fig. 2 for various ratios of  $V_g/V_h$ . We take the radius of the sample  $R$  to be the value at which the density profile extrapolates to zero. We define the width of the profile,  $b_s$ , as the separation of the points where the density is 10% and 90% of the density at the center. The parameters are  $V_g/V_h = 0.5$  and  $b_s = 0.7$  mm for data presented in Figs. 3, 4, 8, and 9, and  $V_g/V_h = 0.8$  and  $b_s = 0.6$  mm for data presented in Figs. 5, 6, and 10. Data are

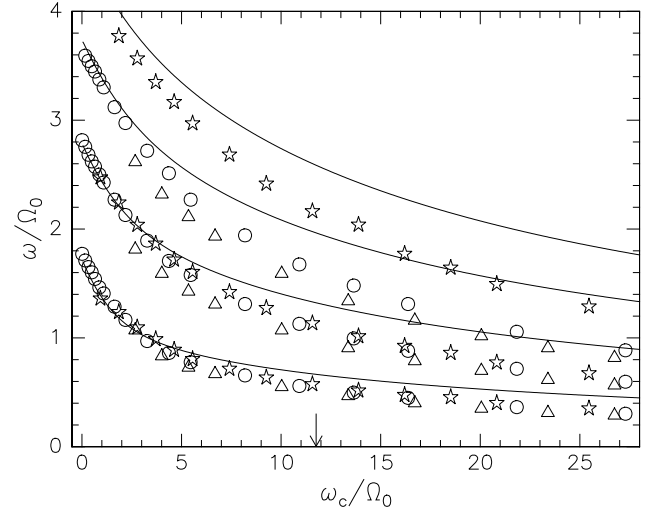


FIG. 3: Normalized mode frequencies versus normalized cyclotron frequency.  $R = 9.8$  mm. Azimuthal modes  $L = 1$ –3: triangles,  $n_{12} = 0.7$ ; circles,  $n_{12} = 1.05$ .  $L = 1, 2$ , and 4: stars,  $n_{12} = 1.46$ .  $\omega_0 = 20.2(n_{12})^{1/2}$  MHz. Frequency and field values range from 5–92 MHz and 0–0.022 T, respectively. Curves represent Fetter's theory for  $L = 1$ –4.

taken between 300 and 400 mK unless indicated. Only the linewidth data are temperature dependent.

## IV. RESULTS

### A. Mode frequencies

In the following graphs arrows on the abscissa indicate the value of  $\omega_c = \omega_0$  or magnetic field at which  $\omega = \omega_0$ . The frequencies probed range from 2.6 to 92 MHz.

The data at small magnetic fields are compared with Fetter's theory [15] in Figs. 3 and 4. The kernel  $K_{ij}$  given in Eq. (6) depends on the screening ratio  $h=R$  but is independent of density. It follows from Eq. (4) that, within the theory of Fetter, for a fixed value of  $h=R$  a normalized plot of  $\omega/\omega_0$  versus  $\omega_c/\omega_0$  is universal. In Fig. 3 normalized data are compared with Fetter's theory for three densities given in units of  $n_{12} = 10^{12} \text{ m}^{-2}$ . Level crossings with modes of the upper branches make it difficult to determine the frequency of EMP modes at small fields for larger  $L$  values. The  $L = 3$  and 4 modes are weakly coupled and missing for some densities. Fetter's theory is plotted for the four lowest EMP modes using a  $25 \times 25$  determinant to solve Eq. (4).

The frequency dependence for three ratios of  $h=R$  is shown in Fig. 4. The theory of Fetter is shown using a  $25 \times 25$  determinant in evaluating Eq. (4) for  $h=R = 0.10$  and a  $15 \times 15$  determinant for  $h=R = 0.13$  and  $0.18$ .

Data are first taken for  $h=R = 0.10$  with the saturated sample above electrodes  $B_1$ ,  $B_2$ , and  $B_3$ . Then repelling voltages are sequentially applied to electrodes  $B_2$  and  $B_3$

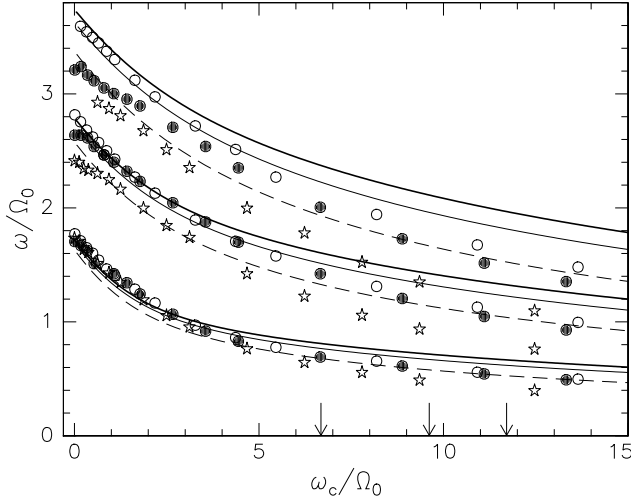


FIG. 4: Normalized m mode frequencies versus normalized cyclotron frequency for  $n_{12} = 1.05$ ,  $L = 1, 3$ , and three ratios of  $h=R$ . Open circles,  $h=R = 0.10$ ; closed circles,  $h=R = 0.13$ ; stars,  $h=R = 0.18$ .  $\omega_0 = 203/R$  (mm) MHz, with  $R$  values of 9.8, 8, and 5.6 mm. The frequency range is 10–74 MHz. The maximum field is 0.016 T. Curves represent Fetter's theory: heavy solid,  $h=R = 0.10$ ; light solid,  $h=R = 0.13$ ; dashed,  $h=R = 0.18$ .

for data sets at  $h=R = 0.13$  and  $0.18$  to insure that the density is the same for the three sets.

Data for a density of  $n_{12} = 0.7$  are compared with the theories of Volkov and Mikhailov [17] for larger magnetic fields in Figs. 5 and 6. Figure 5 is a plot of frequency versus magnetic field. Only data for  $L = 1$  and even modes are shown for clarity. Likewise, theoretical curves, Eq. (12) with  $b = 0.6$  mm and Eq. (13), are shown only for modes 1, 2, 6, and 12. These curves are multiplied by a factor of 0.4. Equation (12) with  $b = 0$  multiplied by a factor of 0.25 is shown for  $L = 1$  and 12.

In Fig. 6 the high-field data are plotted as a function of inverse field in the range  $b \ll b_s$ , where theory predicts  $f \propto B^{-1}$ . The lowest 12 azimuthal modes are shown with the exception of  $L = 7$ . This mode couples weakly, since the rf driving electrode  $T_2$  spans approximately 1.5 wavelengths for this mode. Theoretical curves are shown with the same multiplicative factors used in Fig. 5.

We show the dependence of frequency on the density profile in Fig. 7 for three magnetic field strengths with the sample connected above electrode  $B_1$ . The mode frequency is plotted versus  $jV_g \mp V_h$ . The calculated profile width  $b_s$ , is given on the top axis. This scale is inaccurate below  $b_s = 0.66$  mm. The solid curve shows the variation of  $\omega/R$  from Eq. (12) with  $\omega = b_s$ .

There was no detectable change in the mode frequencies, less than 1%, upon crossing the melting curve.

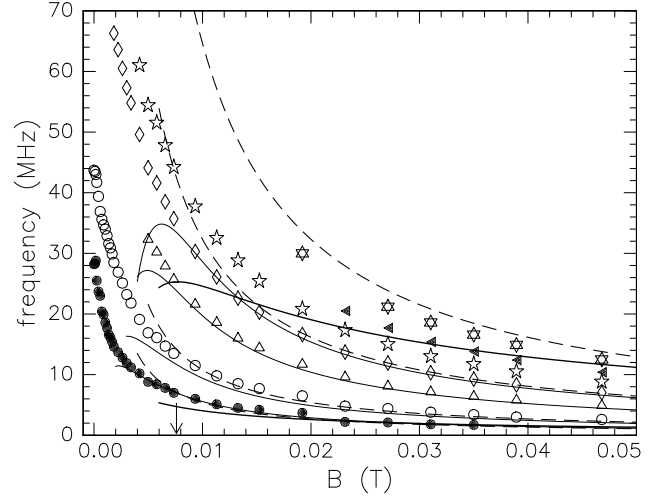


FIG. 5: Frequency versus magnetic field.  $n_{12} = 0.7$ ,  $R = 9.6$  mm. Data are for  $L = 1$  and even modes from  $L = 2$  to 12. Curves represent the theories of Volkov and Mikhailov multiplied by a factor. For modes  $L = 1, 2, 6$ , and 12 with  $b = 0.4$ : none solid, Eq. (12) with  $b = 0.6$  mm; dashed curve, Eq. (13). Bold solid, Eq. (12) with  $b = 0$ ,  $\omega = 0.25$  for  $L = 1$  and 12.

#### B. Linewidths

The signal profiles were Lorentzian, which shows that the modes are not parametrically driven. An example of the derivative signal is shown in the inset of Fig. 8.

The linewidths  $\Delta f = 2$  for three azimuthal quantum numbers are plotted as a function of  $B$  in Fig. 8. The

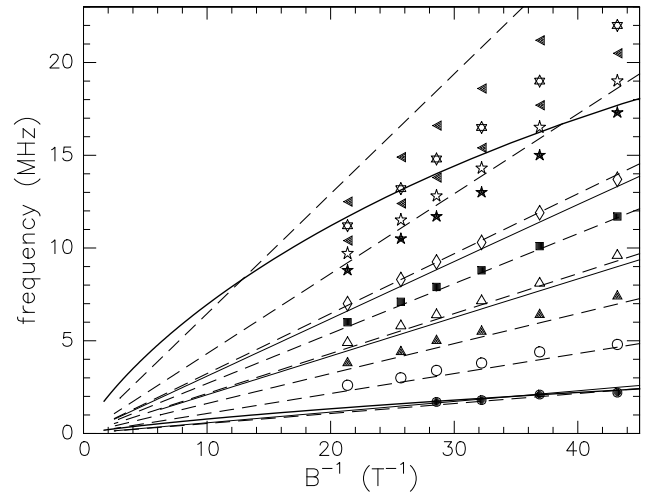


FIG. 6: High-field data plotted as frequency versus inverse field.  $n_{12} = 0.7$ ,  $R = 9.6$  mm. Symbols are for modes  $L = 1, 6, 8, 12$ . Theoretical curves are multiplied by a factor. Light solid, Eq. (12),  $b = 0.6$  mm,  $L = 1, 6$ , and 12; dashed, Eq. (13) for  $L = 1, 6, 8$ , and 12; bold solid,  $b = 0$  for  $L = 1$  and 12; The factors are as labeled in Fig. 5.

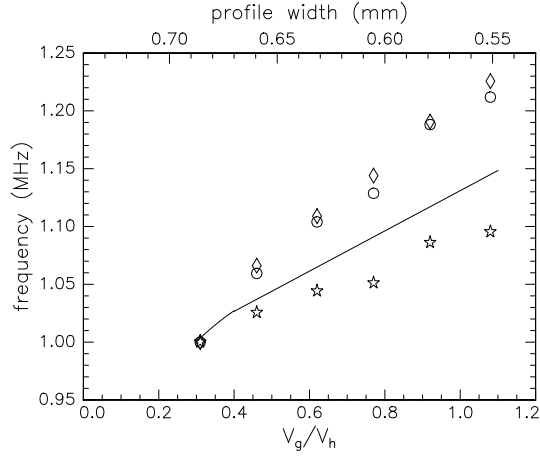


FIG. 7: Frequency versus  $V_g/V_h$ .  $n_{12} = 0.7$ .  $L = 1$ . Stars,  $B = 0$ ; diamonds,  $B = 0.0237T$ ; circles,  $B = 0.0474T$ . Solid curve represents Eq. (12). Both data and theory are normalized to the value at  $V_g/V_h = 0.3$

theoretical linewidths have only a weak dependence on  $L$  through the digamma function in the expression for  $\Gamma_L$ , Eq. (12). The filled symbols represent Eq. (14) for  $L = 1$  with experimental values of the angular frequencies. The value of  $\omega$  is taken from the theory of Vilk and Monarkha.[23] Theoretical values of the linewidths are divided by a factor of 9 to fit the data. The  $Q$ 's of the resonances are approximately  $Q = 5, 9$  and  $17$  for modes  $L = 1, 2$ , and  $4$ , respectively. There is a small increase of about 20% with field over the range plotted in Fig. 8.

Linewidths are shown as a function of temperature in Fig. 9 and compared with theory. Values are included

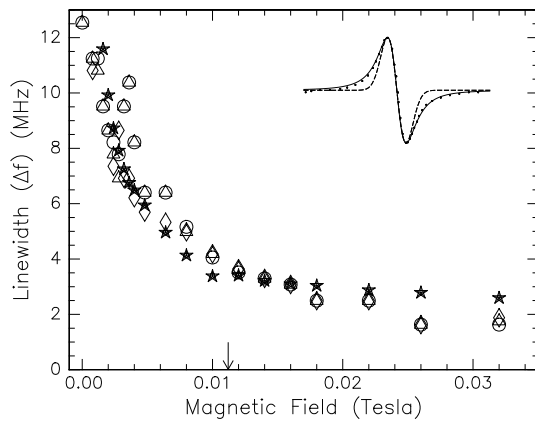


FIG. 8: Linewidth versus magnetic field;  $T = 400$  mK,  $n_{12} = 1.75$ ,  $R = 8$  mm. Symbols: circles,  $L = 1$ ; triangles,  $L = 2$ ; diamonds,  $L = 4$ . Filled symbols represent Eq. (14) for  $L = 1$  with experimental values of  $\Gamma_L$ . Here theoretical values are divided by a factor of 9. Inset: Signal profile. The solid trace is a Lorentzian fit; the dashed trace is a Gaussian fit.

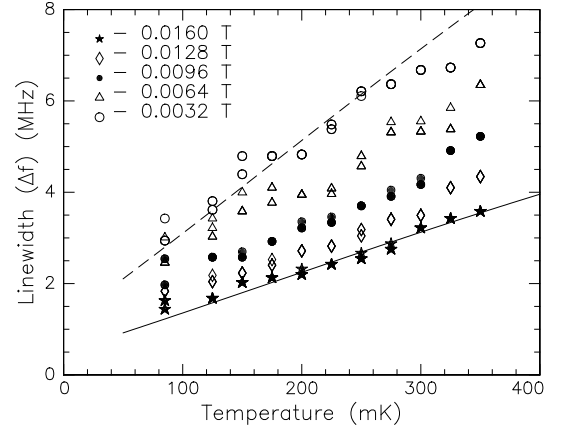


FIG. 9: Linewidth versus temperature for different values of  $B$ .  $n_{12} = 0.88$ .  $R = 9.6$  mm. Identical symbols are used for the lowest four modes. Theoretical curves as explained in the text are dashed line, 32 G; solid line, 160 G.

for the four lowest modes. The curves are given for  $L = 1$  by Eq. (14) divided by a factor of 3 for 32 and 160 G with the experimental value of  $\Gamma_L$  and the theoretical expression [23] for the ripplon-scattering collision time.

### C. Penetration depth

The variation of the penetration depth of the EMP modes with magnetic field can be extracted from the data. The area under the Lorentzian power absorption versus frequency curve is  $P_0/\omega$ , where  $P_0$  is the maximum at the resonant frequency. The area is proportional to the number  $N$  of electrons that participate in the EMP mode and independent of the collision time. The effective number of electrons is

$$N = 2R \int_{-\infty}^{\infty} d\omega \frac{d\epsilon(\omega)}{d\omega} / \epsilon_0 \quad (15)$$

Here  $\omega$  is the coordinate measured from the edge of the sample with an assumed step profile, and  $\omega < R$  is assumed. The magnitude of the extrema in the derivative signal  $S$  is proportional to  $P_0/\omega$ . The penetration depth dependence on field is then

$$(B)/S(\omega)^2 \quad (16)$$

This product  $S(\omega)^2$  is independent of temperature for fixed magnetic field to within the scatter of the data. The product  $S(\omega)^2$  is plotted as a function of magnetic field in Fig. 10. The curves represent  $\epsilon = (\epsilon^2 + b^2)^{1/2}$ ; solid  $-b = 0.6$  mm, dashed  $-b = 0$ .

### V. DISCUSSION

Our data are in close agreement with the theory of Fetter at zero field as observed in Fig. 3. For finite fields



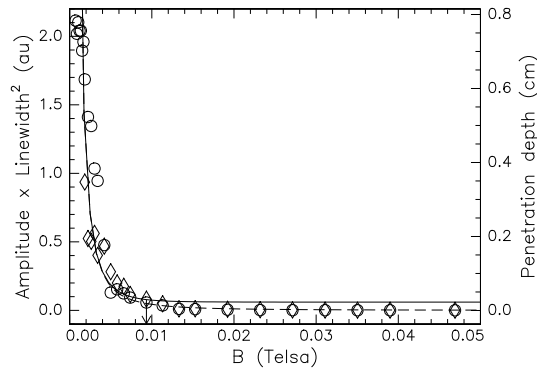


FIG. 10: The product  $S(\Delta)^2$  in arbitrary units versus magnetic field.  $n_{12} = 1.05$ .  $R = 9.6$  mm. Circles,  $L = 2$ ; diamonds,  $L = 5$ . The amplitude for each mode is normalized independently. The solid,  $b = 0.6$  mm, and dashed,  $b = 0$ , curves represent theoretical expressions for the penetration depth (right hand scale).

the data deviate from theory by an amount that increases with magnetic field. The deviation increases with mode number. For data taken at  $n_{12} = 0.7$ , deviation from the two other normalized experimental curves may be due to a loss of electrons.

Fetter's theory assumes a step density profile at the sample edge. Thus it is applicable only for  $\Delta < b$ , where  $\Delta / (\Delta_c = 0)^2$ . The fit of theory to the data is good for the lowest two modes for  $\Delta < 10b$  or  $\Delta_c = 0 < 3$  in Fig. 3. We believe the discrepancy between experiment and theory is not caused by using too few terms in evaluating Eq. (4). The solutions to Eq. (4) using 15 and 25 terms deviate by about 1% at  $\Delta_c = 0 = 15$ . Unfortunately, the range in which we can test this theory is restricted.

The dependence of frequency on the screening parameter  $h=R$ , shown in Fig. 4, is in qualitative agreement with theory, and the separation of curves for different values of  $h=R$  is comparable to that predicted by Fetter. Arrows on the curves indicate the values of  $\Delta_c = 0$  at which  $\Delta = b_s$  with smaller values corresponding to larger ratios of  $h=R$ . The reduced slope for larger values of  $h=R$  and  $L = 2$  and 3 at small fields is not a feature from our data. It may have resulted from an error in identifying the exact frequency for modes  $L$  due to overlap with the upper-branch modes of  $L - 1$ .

The theory of Volkov and Mikhailov, Eq. (12), is compared with the field dependency of our resonant frequencies in the range of applicability,  $B < 10^{-3}$  T, in Figs. 5 and 6. The theory gives the general qualitative behavior of the data. However, the digamma function in the coefficient overly connects the separation between adjacent azimuthal modes. It also gives a decrease in frequency, in contradiction with experiment, for  $\Delta < b_s$ , although this is not a condition for the applicability of this formula.

The data show, particularly in Fig. 6, that ignoring the profile width,  $b = 0$ , gives a poor fit. Setting  $b = 0$

increases the separation of the curves, since it weights the logarithmic term in [Eq. (12)] relative to the digamma function, but does not give the correct curvature as a function of magnetic field. This confirms that the density profile is important in determining the EMP mode frequencies.

We also compare Eq. (13) with our data, although  $b/h = 0.6$  does not satisfy the condition  $b/h < 1$ . It is applicable for  $L = R/h = 10$ . Equation (13), derived for a semi-infinite plane, yields a constant separation between mode frequencies,  $f/L = B$ . A side from a numerical factor, this expression gives a good fit to the data in the range where it is applicable, namely,  $b < \Delta$  and small values of  $L$ . It overestimates the frequency at low magnetic fields due to neglect of the finite sample radius. The theoretical curves are adjusted by a numerical factor of order 2.

The role of the parameter  $b$  is shown explicitly in Fig. 7. The dependence of frequency on the ratio  $j_g/j_{V_h}$  at  $B = 0$  is due to the change in effective sample radius with a change in guard voltage. The frequency ( $f/L = R$ ) changes by 9.5% over the range shown, in agreement with a change in radius of 10%. For the data at larger fields,  $\Delta > b$ , the percent change in frequency with field over the range shown is 23%. We attribute the difference of 13% to a change in  $b$ , which is predicted to be equal to  $b$  in this range. Theoretical frequencies increase by 15% over the range. We note that the definition of  $b$  is somewhat arbitrary, but the theory curve shown in Fig. 7 is nearly insensitive to the definition of  $b$ . We can match the 23% change in the theory only by a increasing the parameter  $b$  by a factor of 10. Not only is this adjustment unphysical, but the change is opposite that needed to improve the fit in Figs. 5 and 6. The decrease in frequency for the lowest value of  $j_g/j_{V_h}$  from an extrapolation of the data at higher ratios is due to the nonlinear dependence of  $R$  and  $b$  on  $j_g/j_{V_h}$  for  $j_g/j_{V_h} < 0.4$ .

The lack of any measurable frequency shift upon crossing the melting curve verifies that the shear modulus has a negligible effect on the dispersion of the EMP modes.

The magnetic-field dependence of the linewidths is in qualitative agreement with theoretical values but differs by a large numerical factor. The data fall below the theory at large fields. The value of  $\Delta$  depends on the electric field, proportional to  $n$ , pressing the electrons to the surface. The theoretical value of  $\Delta$  is 7 ns for  $n_{12} = 1.75$  at 400 mK. For a comparison with experimental values of  $\Delta$ , the theoretical value at 400 mK is 17% less than the experimental value at a density of  $n_{12} = 1.05$ . [24] This does not explain the quantitative discrepancy with theory. The predicted linewidth with the theoretical value of the frequencies is obtained by substituting Eq. (12) into Eq. (14) and is given by  $\Gamma = 1/2$ . This yields a linewidth that is too large by a factor of approximately 5, depending on the field at which experiment and theory are compared, and it also lies above the data at large fields. The temperature dependence of the linewidths agrees with that of ripplon-scattering theory.

The experimental variation of the penetration depth with magnetic field is in agreement with theory for an applicable range of fields. This includes  $B > 0.003$  T, which is the range of validity of Eq. (10),  $!_c^2 / 5!^2$  for  $B = 0.003$  T, and within which the condition  $R$ , assumed in Eq. (15), is satisfied. The assumption of an exponential decay of the wave amplitude may be violated for  $\lambda < b$  or  $B > 0.0094$  T. Note that  $S(!)^2$  is still proportional to the number of electrons participating in the mode, which is shown in Fig. 10 to vanish at large fields.

## VI. CONCLUSIONS

We find that the dependencies of the EM P mode frequencies on magnetic field, azimuthal mode number, and the screening parameter  $h/R$  have the general qualitative behavior predicted by Fetter. Quantitative differences for the lowest modes are small in the range of application of this theory, which is limited.

The data exhibit the qualitative features of the theory of Volkov and Mikhailov. The coefficient in Eq. (12) overly connects the separation of azimuthal modes and at low fields leads to a reduction in frequency in contradiction with experimental data. An adaptation of their theory for a semi-infinite plane to a circular sample fits our data for large fields and small azimuthal mode number. Our data on mode frequencies confirm that the penetration depth is determined by the density profile at large fields as predicted by these authors and Nazin and Shikin. We demonstrate a variation of frequency with a

change of edge density profile.

The magnetic field dependence of EM P linewidths is in qualitative agreement with theory to within the scatter in the data. Experimental linewidths deviate from theory at large fields. Theory and experiment differ by a numerical factor of 9. At large fields the linewidth is independent of mode number as predicted. The temperature variation of the linewidth is in agreement with theory.

We are able to extract the dependence of the penetration depth on magnetic field, assuming an exponential decay of the mode amplitude into the sample. This assumption may not apply when the penetration depth is less than the density profile width. We show that the number of electrons participating in the EM P wave vanishes at large fields. A more exact definition of the profile width would be helpful as well as a prediction of the decay of the EM P amplitude from the sample edge within the profile width.

At our largest azimuthal modes,  $L = 12$ , the wavelength is  $\lambda \approx R/2$ . It would be interesting to investigate higher modes in a sample of larger radius with  $R$  to test theories of the propagation of EM P modes in a semi-infinite sample [4, 17].

## VII. ACKNOWLEDGMENTS

The authors wish to acknowledge M. I. Dykman, A. L. Fetter and Harsh Mathur for helpful conversations. This work was supported in part by NSF grant No. DMR-0071622. M. I. G. wishes to thank the Turkish Ministry of Education for support.

- 
- [1] D. B. Mast and A. J. Dahm, *Physica* 126 B & C 457 (1984).
  - [2] D. B. Mast, A. J. Dahm, and A. L. Fetter, *Phys. Rev. Lett.* 54, 1706 (1985).
  - [3] D. C. Glatli, E. Y. Andrei, G. Deville, J. Poitrenaud, and F. I. B. Williams, *Phys. Rev. Lett.* 54, 1710 (1985).
  - [4] S. J. Allen, H. L. Stormer, and J. C. M. Hwang, *Phys. Rev. B* 28, 4875 (1983).
  - [5] D. C. Glatli, E. Y. Andrei, G. Deville, and F. I. B. Williams, *Surf. Sci.* 170, 70 (1986).
  - [6] P. J. M. Peters, M. J. Lea, A. M. L. Janssen, A. O. Stone, W. P. N. M. Jacobs, P. Fozooni, and R. W. van der Heijden, *Phys. Rev. Lett.* 67, 2199 (1991).
  - [7] Y. P. Monarkha, S. Ito, K. Shirahama, and K. Kono, *Phys. Rev. Lett.* 78, 2445 (1997).
  - [8] P. K. H. Sommerfeld, P. P. Steijaert, P. J. M. Peters, and R. W. van der Heijden, *Phys. Rev. Lett.* 74, 2559 (1995).
  - [9] O. I. Kirichek, P. K. H. Sommerfeld, Y. P. Monarkha, P. J. M. Peters, Y. Z. Kovdyra, P. P. Steijaert, R. W. van der Heijden, and A. T. A. M. de Waele, *Phys. Rev. Lett.* 74, 1190 (1995).
  - [10] P. K. H. Sommerfeld, A. T. M. Valkering, R. W. van der Heijden, and A. T. A. M. de Waele, *Surf. Sci.* 361/362 839, (1996).
  - [11] O. I. Kirichek, I. B. Berkutov, Y. Z. Kovdyra, and V. N. Grigor'ev, *J. Low Temp. Phys.* 109, 397 (1997).
  - [12] P. L. Elliott, C. I. Pakes, L. Skibek, and W. F. Vinen, *Phys. Rev. Lett.* 75, 3713 (1995).
  - [13] A. L. Fetter, *Phys. Rev. B* 32, 7676 (1985).
  - [14] A. L. Fetter, *Phys. Rev. B* 33, 3717 (1986).
  - [15] A. L. Fetter, *Phys. Rev. B* 33, 5221 (1986).
  - [16] V. A. Volkov and S. A. Mikhailov, *Pis'ma Zh. Eksp. Teor. Fiz.* 42, 450 (1985) [*JETP Lett.* 42, 556 (1985)].
  - [17] V. A. Volkov and S. A. Mikhailov, *Zh. Eksp. Teor. Fiz.* 94, 217 (1988) [*Sov. Phys. JETP* 67, 1639 (1988)].
  - [18] V. A. Volkov and S. A. Mikhailov, in *Modern Problems in Condensed Matter Sciences*, edited by V. M. Agnovich and A. A. Maradudin (North-Holland, Amsterdam, 1991), Vol. 27.2, Chap. 15, p. 855.
  - [19] S. S. Nazin, N. I. Shikina, and V. B. Shikin, *Zh. Eksp. Teor. Fiz.* 92, 1648 (1987) [*Sov. Phys. JETP* 65, 924 (1987)].
  - [20] S. S. Nazin and V. B. Shikin, *Zh. Eksp. Teor. Fiz.* 94, 133 (1988) [*Sov. Phys. JETP* 67, 288 (1988)].
  - [21] M. I. Goksu, M. okyang Kim, M. T. Chen, K. A. Mantey, J. A. Castiglione, and A. J. Dahm, *Physica B* 329-333, 268 (2003).
  - [22] M. I. Goksu and A. J. Dahm, *J. Low Temp. Phys.* 134,

553 (2004).

- [23] Y. M. Vilk and Y. P. Monarkha, *Fiz. Nizk. Temp.* 15, 235 (1989) [*Sov. J. Low Temp. Phys.* 15, 131 (1989)].
- [24] R. M. Mehrotra, C. J. Guo, Y. Z. Ruan, D. B. Mast, and A. J. Dahm, *Phys. Rev. B* 29, 5239 (1984).